J. Appl. Comput. Mech., 10(3) (2024) 597–609
DOI: 10.22055/jacm.2024.45899.4427

ISSN: 2383-4536
jacm.scu.ac.ir

Shahid Chamran University of Ahvaz

Journal of Applied and Computational Mechanics

Research Paper

Enhanced Flow and Temperature Profiles in Ternary Hybrid Nanofluid with Gyrotactic Microorganisms: A Study on Magnetic Field, Brownian Motion, and Thermophoresis Phenomena

Ahmed S. Rashed[1,2], Tarek A. Mahmoud[1], Samah M. Mabrouk[1]

[1] Department of Physics and Engineering Mathematics, Faculty of Engineering, Zagazig University, Zagazig, 44515, Egypt,
Email: ahmed.s.rashed@gmail.com (A.S.R.); tamibrahim@eng.zu.edu.eg (T.A.M.); samahmm@gmail.com (S.M.M.)

[2] Faculty of engineering, Delta University for Science and Technology, Gamasa, Egypt

Received January 20 2024; Revised March 12 2024; Accepted for publication March 16 2024.
Corresponding author: A.S. Rashed (ahmed.s.rashed@gmail.com)

Abstract. This innovative study investigates the flow of ternary hybrid nanofluid containing gyrotactic microorganisms in microchannel. The magnetic field, thermophoresis, and Brownian motion effects are analyzed. The transformation of the PDEs system into ODEs is carried out by using the group transformation method. The innovative findings examine the Newtonian and non-Newtonian models derived from the system of ODEs. Several graphs illustrate how different parameters affect the velocity profile, temperature, concentration, and microorganisms. The power-law index value increases the fluid flow velocity by about 9% at $n = 3$, 36% at $n = 4$ relative to the case of $n = 2.5$ at the center of the boundary layer. Moreover, the ternary hybrid nanofluid exhibits a greater temperature compared to the nanofluid. The current results are compared to the researchers' findings to confirm the validity of the obtained results. When the Prandtl number is between 6 and 10, the Nusselt number reaches 45.49%.

Keywords: Microchannel; Bioconvection; Inclined configuration; Power- law index; Solar radiation; Ternary hybrid nanofluid.

1. Introduction

Solar energy is a natural resource which produces energy without burning any fuel, so it can be considered as the best choice because it is clean [1]. A renewable energy source is solar energy which accomplishes the demands of energy in industrial and technical applications. Solar energy is the result of chemical processes that convert solar radiation into heat or electricity [2].The heat transfer property of a fluid within the geometry is essential in thermal systems like heat exchangers, micro technological apparatus and solar panels. The heat and mass transfer inside microchannel have requisite interest owing to its applicability in engineering field like turbo machinery, mixing of samples, refrigeration process, solar panels, solar absorption and solar cells [3, 4]. Fakour et al. [5] examined the nanofluid flow in a vertical channel with existence of buoyancy force. The results indicated that the nanoparticle volume fraction profiles were strongly related against the Grashof number (Gr). Acharya et al. [6] scrutinized the influence of aggregation kinetics of nanofluid through the microchannel. He stated that the thermal conductivity of the composite enhances with higher values of the concentration of nanoparticles. Heat transport decreases with the radius of gyration factor in the lower segment but increases in the upper region.

The ternary hybrid nanofluid (THNF) consists of nanoparticles with various physical and chemical properties to the base fluid. The author showed that the temperature profile was raised as the Prandtl number grew. Increasing the thermal relaxation value decreases the thermal distribution profile [7]. Ternary hybrid nanofluid has high thermal conductivity which enhances heat transmission and efficiency of solar system [8]. Bilal et al. [9] studied the thermal enhancement of (TiO_2-$CoFe_2O_4$-MgO/H_2O) nanofluid through cone, wedge and sheet. Cone surfaces have higher velocity and energy propagation rates than wedges and plates, regardless of heat source or porosity effect. However, a wedge surface has a higher mass transfer ratio when impacted by activation energy compared to a plate. Alqawasmi et al. [10] investigated the thermal radiation of THNF around disk with influence of normal magnetic field. The scientists found that decreasing magnetic parameter values leads to decreased fluid velocity and increased fluid temperature across the disk. For higher values, the temperature and radiant heat components enhances. The ternary composite nanofluid has the highest influence on the surface. Mohanty et al. [11] studied the heat transmission of THNF through a vertical cylinder with the effect of heat source. The study found that improving the Brinkman and radiation parameters leads to a nonlinear decrease in entropy production, whereas improving the Bejan number results in an opposite procedure.

Bioconvection is described as the swimming of a microorganism in a specified direction which is weightier than water as a result of this a gradient of density will appear contributing the forming of convective motion [12]. Researchers discovered that increasing the temperature ratio parameter leads to an augment in temperature field, whereas rising the Prandtl number causes a diminish in temperature field. Furthermore, temperature-dependent heat source parameters raise fluid temperatures. The

Published online: March 30 2024

nanoparticles concentration diminishes with enhancing Lewis number. The microorganism profile decays due to an increase in the Peclet number. Jawad et al. [13] analyzed the induced magnetic field over a horizontal sheet with hybrid nanofluid (HNF) containing gyrotactic microorganisms. Shah et al. [14] described bioconvection flow with activation energy using the mathematical model. The study found that raising the magnetic field parameter resulted in decreased porosity factor velocity profiles. As the couple-stress parameter increases, the velocity profile follows suit.

Rashed et al. [15, 16] introduced a mathematical model to study the behavior of nanofluid around vertical plate and cylindrical solid pipes, respectively. Mabrouk et al. [17] examined the power index and its effects on the hybrid nanofluid inside solar collector. They concluded that the velocity is improved with the boosting of power – law index. The same authors in [18] introduced entropy and thermal behavior of solar energy in water solar collector. They stated that raising the inclination angle results in raising the temperature but lowering the fluid velocity.

Abdollahi et al. [19] presented the performance of heat transmission of hybrid nanofluids in a parallel surface. The study found that increasing the Reynolds number reduces heat transfer and decreases heat fluxes from surfaces, resulting in lower nanofluid flow rates. On the other hand, the nanoparticles concentration rises with the Reynolds number. Chu et al. [20] stated that the microorganisms distribution was diminished with the incrementation of Peclet number *Pe*. The authors stated that improved velocity profile leads to better wedge angle parameters for static and moving wedges. Falkner-Skan nanofluid velocity decreased with increasing infinite shear rate viscosity, bioconvection Rayleigh number, and buoyancy ratio. The singular manifolds method and Lie infinitesimals were employed to solve some fluid dynamic applications [21-23] and evolution equations [24, 25], respectively. Sarma and Paul [26] studied bioconvection in a cylindrical Ag-CuO/H_2O Ellis hybrid nanofluid with bacteria around stretched cylindrical tube. The observations showed that the Ellis fluid parameter increases velocity while decreasing temperature and concentration profiles. In contrast, thermophoresis and Brownian motion increase the rates of mass transfer, whereas slip has the reverse effect. Peclet number and bioconvective constants show interesting but opposing tendencies with gyrotactic microbe profiles, providing valuable insights. Paul et al. [27] studied the mixed convection due to the presence of HNF through across a radiative cone. The study found that Casson nanofluid significantly improved tangential skin friction by 52%. The thermal performance of MHD flow of Al_2O_3-Cu-TiO_2/HO_2 has been examined by Rafique et al. [28]. The researchers discovered that increasing magnetic parameters points to a decrease in temperature and an increase in velocity. Moreover, Paul et al. [29] analyzed the unsteady Casson-Maxwell hybrid nanofluids in case of variable thermal conductivity. The results indicated that merging the Casson and Maxwell HNF resulted in significant improvements in skin friction: heat transmission increased by percentage of 11% relative compared to the Casson-Maxwell nanofluid. Mahmood et al. [30] presented a numerical analysis for a tri-hybrid nanofluid around sheet. Islam et al. [31] examined the electroosmotic flow incorporating ternary hybrid nanoparticles. The thermo-migration factor shows a decline in mass transport rate. The Peclet number reduces the density of motile microbes. Also, Islam et al. [32] analyzed the dynamics of Carreau nanomaterial flow in case of chemical reaction. The studies revealed that the changed Hartmann number improves the mobility of nanomaterials. The radiation variable produces the opposite outcomes in terms of heat transport rate and entropy. Rana et al. [33, 34] examined the entropy optimized nano-bioconvective flow and microbes in blood flow. The results showed that the blood velocity decreases as the Williamson factor increases and increases with the viscosity ratio. Islam et al. [35] presented a numerical analysis to study MHD flow. A greater Rayleigh number and concentration of nanoparticles improved the thermal enactment of hybrid nanofluid. Reverse behaviors should be noticed when the magnetic impact increases. The nanofluids could be used as mono, hybrid, and Ternary hybrid nanofluids. The concept behind these types is to have the benefits of different nanoparticles instead of mono type. Samrity and Yin [36] investigated the performance of pulsating heat pipe. The results revealed that the Al_2O_3-Cu HNF reached to 30-54% lower thermal resistance than water at the same filling ratio and heat input, indicating improved heat transfer. From the literature, there are not any previously attempts have been made to investigate the three-dimensional bio-convection flow of ternary hybrid nanofluid inside the inclined microchannel. Therefore, the motivation of these investigations deals with the three-dimensional flow during the influence of solar radiation as well as magnetic field.

The novel work includes:

a. Obtaining the flow and thermal characteristics of Newtonian (n = 2) and non-Newtonian ($n \neq 2$) models from the resulting system of ODEs, to handle various cases of operation.
b. Increasing the power-law index resulting in improving in the velocity and temperature of ternary hybrid nanofluid which signifies that the overall thermal system efficiency has been enhanced.

In the applied method, the system of ODEs is achieved at cases of power-law index (n = 2 and $n \neq 2$). Moreover, the optimal value of power-law index at which the higher value of velocity and temperature of ternary hybrid nanofluid happens, has been chosen prominently by various graph, unlike the conventional method used by other researchers as in [2, 37]. As a result, the applied method GTM has no limitations and represents a novel form of the related mathematical methods mentioned in [15, 38, 39].

2. Mathematical Formulation

In the present work, three-dimensional flow has been considered incorporating incompressible ternary hybrid nanofluid containing microorganisms, non-Newtonian and unsteady state fluid dynamics. In a microchannel, the ternary hybrid nanofluid flow between two revolving parallel surfaces with angular velocity $\Omega = (0, \Omega, 0)$. The plates are placed at y = 0 and $y = h$. This study considers the upper plate moves with v_w, while lower plate moves with stretching speed u_w. Moreover, the temperature of the lower segment is T_w and the upper portion is at T_0. For efficient flow control, the magnetic field is applied in y-direction. Figure 1 shows the structure of the present model. Based on above conditions, the model equations can be expressed as [2, 4, 6, 40]:

$$u^*_x + v^*_y + w_z = 0, \tag{1}$$

$$u^*_t + u^* u^*_x + v^* u^*_y + 2\Omega w - \nu_{thnf}\left(u^*_{xx} + u^*_{yy}\right)^{n-1} + \frac{1}{\rho_{thnf}} P^*_x + \left(\frac{\sigma_{thnf} B_0^2}{\rho_{thnf}}\right) u^* \sin^2(\Gamma) = 0, \tag{2}$$

$$w_t + u^* w_x + v^* w_y - 2\Omega u^* - \nu_{thnf}\left(w_{xx} + w_{yy}\right)^{n-1} + \left(\frac{\sigma_{thnf} B_0^2}{\rho_{thnf}}\right) w \sin^2(\Gamma) = 0, \tag{3}$$

$$v^*_t + u^* v^*_x + v^* v^*_y - \nu_{thnf}\left(v^*_{xx} + v^*_{yy}\right)^{n-1} + \frac{1}{\rho_{thnf}} P^*_y = 0, \tag{4}$$

$$\left(T_t + u^* T_x + v^* T_y + w T_z\right) - \left(\alpha_{thnf} + \frac{16\sigma^* T_\infty^3}{3k^*\left(\rho c_p\right)_{thnf}}\right) T_{yy} - \nu_{thnf} v_y^{*2} = 0, \tag{5}$$

$$C_t^* + u^* C_x^* + v^* C_y^* + w C_z^* = D_B\left(C_{xx}^* + C_{yy}^* + C_{zz}^*\right) + \frac{D_T}{T_\infty}\left(T_{xx} + T_{yy} + T_{zz}\right), \tag{6}$$

$$N_t + u^* N_x + v^* N_y + w N_z + \frac{\chi W_c}{\left(C_w - C_\infty\right)}\left(\frac{\partial}{\partial x}\left(NC_x^*\right) + \frac{\partial}{\partial y}\left(NC_y^*\right) + \frac{\partial}{\partial z}\left(NC_z^*\right)\right) = D_n\left(N_{xx} + N_{yy} + N_{zz}\right) \tag{7}$$

where (u^*, v^*, w) are the flow speed along coordinate axes (x, y, z), respectively, Ω denotes the angular velocity, p^* denotes the fluid pressure, T^* represents the temperature, C^* is the concentration of nanoparticles, t is the time, χ denotes the chemotaxis constant, W_c refers to swimming speed, D_T, D_B and D_n are the coefficients of thermophoresis, Brownian diffusion and microorganisms diffusion, respectively. Also, the subscripts *f* and *thnf* referred to the base fluid and ternary hybrid nanofluid. The boundary conditions are [4, 19]:

$$\begin{aligned} &u^* = u_w, v^* = 0, w = 0, p^* = p_w, T = T_w, C^* = C_w, N = N_w \rightarrow y = 0 \\ &u^* = 0, v^* = v_w, w = 0, p^* = p_0, T = T_0, C^* = C_0, N = N_0 \rightarrow y = H \end{aligned} \tag{8}$$

The dependent variables are introduced in the normalized form as [41, 42]:

$$u(x,y,z,t) = \frac{u^*(x,y,z,t)}{u_w(x,z,t)}, v(x,y,z,t) = \frac{v^*(x,y,z,t)}{v_w(x,y,t)}, p = \frac{P^*(x,y,z,t)}{p_w(x,z,t)}, \theta = \frac{T - T_0}{T_w - T_0}, C = \frac{C^* - C_0}{C_w - C_0}, \psi = \frac{N - N_0}{N_w - N_0} \tag{9}$$

Consequently, Eqs. (1) to (6) become as follows:

$$u_x u_w + u\left(u_w\right)_x + v_y v_w + v\left(v_w\right)_y + w_z = 0, \tag{10}$$

$$u_t u_w + u\left(u_w\right)_t + u u_w\left(u_x u_w + u\left(u_w\right)_x\right) + v v_w u_w u_y + 2\Omega w - \nu_{thnf}\left(u_w\left(u_{xx} + u_{yy}\right)\right)^{n-1} + \frac{1}{\rho_{thnf}}\left(p_x p_w + p\left(p_w\right)_x\right) + \left(\frac{\sigma_{thnf} B_0^2}{\rho_{thnf}}\right)\sin^2(\Gamma) u u_w = 0, \tag{11}$$

$$w_t + u u_w w_x + v v_w w_y - 2\Omega u u_w - \nu_{thnf}\left(w_{xx} + w_{yy}\right)^{n-1} + \left(\frac{\sigma_{thnf} B_0^2}{\rho_{thnf}}\right)\sin^2(\Gamma) w = 0, \tag{12}$$

$$v_t v_w + v\left(v_w\right)_t + u u_w\left(v_x v_w + v\left(v_w\right)_x\right) + v v_w\left(v_y v_w + v\left(v_w\right)_y\right) - \nu_{thnf}\left(v_w\left(v_{xx} + v_{yy}\right)\right)^{n-1} + \left(p_y p_w + p\left(p_w\right)_y\right) = 0, \tag{13}$$

$$\Delta T\left(\theta_t + u u_w \theta_x + v v_w \theta_y + w\theta_z\right) - \Delta T\left(\alpha_{thnf} + \frac{16\sigma^* T_\infty^3}{3k^*\left(\rho c_p\right)_{thnf}}\right)\theta_{yy} - \frac{\mu_{thnf}}{\left(\rho c_p\right)_{thnf}} v_y^2 = 0. \tag{14}$$

$$\Delta C\left(C_t + u u_w C_x + v v_w C_y + w C_z\right) - \Delta C D_B\left(C_{xx} + C_{yy} + C_{zz}\right) - \frac{\Delta T D_T}{T_0}\left(\theta_{xx} + \theta_{yy} + \theta_{zz}\right) = 0. \tag{15}$$

$$\Delta N\left(\psi_t + u u_w \psi_x + v v_w \psi_y + w\psi_z\right) + \frac{\chi W_c}{\left(C_w - C_0\right)}\left(\frac{\partial}{\partial x}\left(\left(\Delta N\psi + N_0\right)\Delta C C_x\right) + \frac{\partial}{\partial y}\left(\left(\Delta N\psi + N_0\right)\Delta C C_y\right) + \frac{\partial}{\partial z}\left(\left(\Delta N\psi + N_0\right)\Delta C C_z\right)\right) = D_n \Delta N\left(\psi_{xx} + \psi_{yy} + \psi_{zz}\right). \tag{16}$$

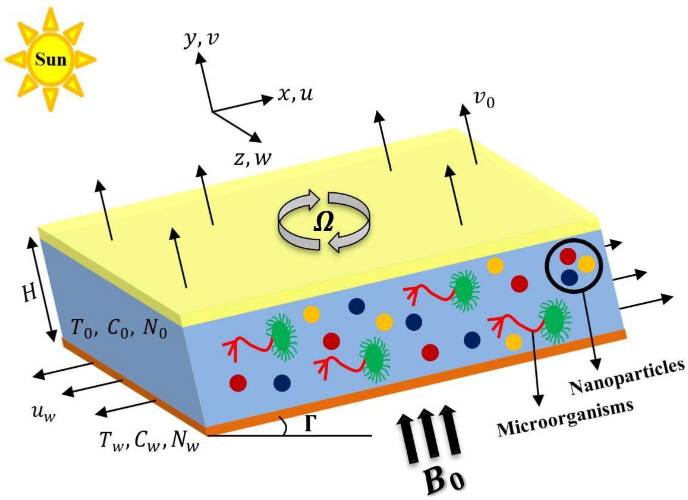

Fig. 1. Schematic configuration of the considered system.

The associated boundary conditions are defined as:

$$\begin{aligned} &u=1, v=0, w=0, p=1, \theta=1, C=1, \psi=1 \to y=0 \\ &u=0, v=1, w=0, p=0, \theta=0, C=0, \psi=0 \to y=H \end{aligned} \tag{17}$$

3. Group Transformation Method (GTM)

The GTM is employed to the system's equations (10) to (16). The PDEs will be converted to ODEs by applying the GTM.

3.1. Group systematic formulation of the system

The GTM is defined as follows:

$$\bar{S} = Q^{s}(a_1, a_2, a_3)S + K^{s}(a_1, a_2, a_3). \tag{18}$$

where, S refers to the system variables, Q^s and K^s indicate the function to be differentiable in each of three parameters; a_1, a_2 and a_3. The partial derivatives of the system are stated as:

$$\left.\begin{aligned} \bar{S}_{\bar{i}} &= \left(\frac{Q^s}{Q^i}\right) S_i \\ \bar{S}_{\bar{i}\,\bar{j}} &= \left(\frac{Q^s}{Q^i Q^j}\right) S_{ij} \end{aligned}\right\}, \; i = x, y, z, t \text{ and } j = x, y, z, t. \tag{19}$$

Extending the same procedures described in details as in Morgan's theorem [43] leads to achieve the transformations of the following variables x, y, z, t; u, v, w, u_w, v_w, p_w, p, θ, C, ψ, now we can get:

$$\eta(x, y, z, t) = y\varepsilon(x, z, t) \tag{20}$$

where $\varepsilon(x,z,t)$ will be found later. The dependent variables in the transformed form give the similarity variables, which will be:

$$\begin{cases} u = U(x,z,t) f(\eta) \\ w = W(x,z,t) h(\eta) \\ v = g(\eta) \\ p = \zeta(x,z,t) E(\eta) \\ \theta = \xi(x,z,t) \Theta(\eta) \\ C = \varrho(x,z,t) \phi(\eta) \\ \psi = \pi(x,z,t) \Psi(\eta) \\ u_w = u_w(x,z,t) \\ v_w = v_w(x,y,t) \\ p_w = p_w(x,z,t) \end{cases} \tag{21}$$

Using these transformations reduces the system of equations (10) to (16) to the new system:

$$u_w U_x f + u_w U \varepsilon_x \eta f' + U (u_w)_x f + v_w \varepsilon g' + (v_w)_y g + W_z h + W_y \varepsilon_z h' + Wh = 0, \tag{22}$$

$$\begin{aligned} &-\nu_{thnf} \left(\varepsilon^2\right)^{n-1} \left(f''\right)^{n-1} + \left(\frac{(u_w)_t}{U^{n-2} u_w^{\,n-1}} + \frac{U_t}{U^{n-1} u_w^{\,n-2}}\right) f + \left(\frac{y\varepsilon_t}{(Uu_w)^{n-2}}\right) f' + \left(\frac{(u_w)_x}{U^{n-3} u_w^{\,n-2}} + \frac{U_x}{U^{n-2} u_w^{\,n-3}}\right) f^2 + \frac{y\,\varepsilon_x}{(Uu_w)^{n-3}} ff' + \frac{v_w \varepsilon}{(Uu_w)^{n-2}} gf' \\ &+ 2\Omega \frac{W}{(Uu_w)^{n-1}} h + \frac{1}{\rho_{thnf}} \left(\left(\frac{\left(p_w \zeta_x + \zeta (p_w)_x\right) E + \left(p_w \zeta y\, \varepsilon_x\right) E'}{(Uu_w)^{n-1}}\right)\right) + \frac{1}{(Uu_w)^{n-2}} \left(\frac{\sigma_{thnf} B_0^2}{\rho_{thnf}}\right) \sin^2(\Gamma) f = 0, \end{aligned} \tag{23}$$

$$-\nu_{thnf} \left(\varepsilon^2\right)^{n-1} \left(h''\right)^{n-1} + \left(\frac{W_t}{W^{n-1}}\right) h + \left(\frac{Uu_w (\varepsilon_x / \varepsilon)}{(W)^{n-2}}\right) h' + \left(\frac{Uu_w W_x}{W^{n-1}} + \frac{Uu_w}{W^{n-2}}\right) fh + \left(\frac{v_w \varepsilon}{(W)^{n-2}}\right) gh' - 2\Omega \frac{Uu_w}{(W)^{n-1}} f + \frac{1}{(W)^{n-2}} \left(\frac{\sigma_{hnf} B_0^2}{\rho_{hnf}}\right) \sin^2(\Gamma) h = 0, \tag{24}$$

$$-\nu_{thnf} \left(\varepsilon^2\right)^{n-1} \left(g''\right)^{n-1} + \left(\frac{\varepsilon}{(v_w)^{n-3}}\right) gg' + \frac{1}{\rho_{thnf}} \left(\frac{p_w \zeta \varepsilon}{(v_w)^{n-1}}\right) E' = 0, \tag{25}$$

$$-\left(\alpha_{thnf} + \frac{16\sigma^* T_\infty^3}{3k^* \left(\rho c_p\right)_{thnf}}\right) \Delta T \Theta'' + \Delta T \left[\left(\frac{\xi_t}{\xi \varepsilon^2}\right) \Theta + \left(\frac{\varepsilon_t}{\varepsilon^2}\right) \Theta' + u_w U \left(\frac{\xi_x}{\xi \varepsilon^2} f\Theta + \frac{1}{\varepsilon} f\Theta'\right) + v_w \left(\frac{1}{\varepsilon} \Theta'\right) + W \left(\left(\frac{\xi_z}{\xi \varepsilon^2}\right) h\Theta + \frac{1}{\varepsilon} h\Theta'\right)\right] - \left(\frac{\mu_{thnf}}{\Delta T \, \rho c_p)_{thnf}}\right) \frac{(v_w)^2}{\xi} g'^2 = 0, \tag{26}$$

$$-\Delta C\phi'' - \Delta T\frac{D_T}{T_o D_B}\left(\frac{\xi}{\varrho}\right)\Theta'' + \Delta C\left[\left(\frac{\varrho_t}{\varrho\varepsilon^2}\right)\phi + \left(\frac{y\varepsilon_t}{\varepsilon^2}\right)\phi' + u_w U\left(\left(\frac{\varrho_x}{\varrho\varepsilon^2}\right)f\phi + \left(\frac{\varepsilon_x y}{\varepsilon^2}\right)f\phi'\right) + \upsilon_w\frac{1}{\varepsilon}g\phi' + W\left(\left(\frac{\varrho_z}{\varrho\varepsilon^2}\right)h\phi + \left(\frac{\varepsilon_z y}{\varepsilon^2}\right)h\phi'\right)\right] = 0, \tag{27}$$

$$\begin{aligned}&-D_n\Delta N\Psi'' - \Delta N\left[\left(\frac{\pi_t}{\pi\varepsilon^2}\right)\Psi + \left(\frac{Uu_w\pi_x}{\pi\varepsilon^2}\right)f\Psi + \left(\frac{\upsilon_w}{\varepsilon}\right)g\Psi' + \left(\frac{W\pi_z}{\pi\varepsilon^2}\right)f\Psi\right] + \chi W_c\Delta N\left(\left(\left(\frac{\varrho_x}{\pi\varepsilon^2}\right)\phi + \left(\frac{\varrho y\varepsilon_x}{\pi\varepsilon^2}\right)\phi'\right)\left(\left(\frac{\pi_x}{\pi\varepsilon^2}\right)\Psi + \left(\frac{y\varepsilon_x}{\varepsilon^2}\right)\Psi'\right) + \right.\\ &\left.\varrho\left(\pi\Psi\phi'' + \left(\frac{N_\infty}{\Delta N}\right)\left(\frac{1}{\pi}\right)\phi'' + \Psi'\phi'\right) + \left(\left(\frac{\varrho_z}{\pi\varepsilon^2}\right)\phi + \left(\frac{\varrho y\varepsilon_z}{\pi\varepsilon^2}\right)\phi'\right)\left(\left(\frac{\pi_z}{\pi\varepsilon^2}\right)\Psi + \left(\frac{y\varepsilon_z}{\varepsilon^2}\right)\Psi'\right)\right) = 0.\end{aligned} \tag{28}$$

The functions of $u_w, \upsilon_w, p_w, U(x, z, t), W(x, z, t), \zeta(x, z, t), \xi(x, z, t), \varrho(x, z, t), \pi(x,z,t)$ and $\eta(x, y, z, t)$ will be accurately calculated such that the equations (10) to (16) can now be reduced to ODEs. The two cases of power-law index will be taken into consideration.

Case-1; (*n* = 2) for a case of Newtonian model

As a result, the functions take the form:

$$u_w = bx, \upsilon_w = \upsilon_o bH, U = u_o\nu_f, W = bu_o\nu_f^{\,2}x, p_w = e^{-(\nu_f x)^2}, \zeta = e^{+(\nu_f x)^2}, \xi = \varrho = \pi = \frac{1}{\sqrt{b\nu_f}}\, and \quad \eta = y\frac{\nu_f}{H} \tag{29}$$

From the previous results in Eq. (29), the system (22) to (28) will be shown as:

$$f'' - \varepsilon_6\left(u_o Rf^2 + \upsilon_o Rgf' + 2\lambda h + M\left(\frac{\varepsilon_5}{\varepsilon_2\varepsilon_6}\right)Rf\sin^2(\Gamma)\right) = 0, \tag{30}$$

$$h'' - \varepsilon_6\left(u_o Rfh + \upsilon_o Rgh' - \left(\frac{2\lambda}{\nu_f^{\,2}}\right)f + M\left(\frac{\varepsilon_5}{\varepsilon_2\varepsilon_6}\right)Rh\sin^2(\Gamma)\right) = 0, \tag{31}$$

$$g'' - \left(\frac{1}{\nu_{thnf}}\right)\left(Rgg' + \left(\frac{1}{\upsilon_o\rho_{thnf}\varepsilon_3}\right)E'\right) = 0, \tag{32}$$

$$\Theta'' + \left(\frac{RPr}{\varepsilon_4 + PrR_d}\right)\left(\varepsilon_3\varepsilon_7 g\Theta' - \left(\frac{\varepsilon_1\varepsilon_6}{\Delta T}\right)g'^2\right) = 0, \tag{33}$$

$$\Phi'' + \left(\frac{N_t}{N_b}\right)\Theta'' - R\left(\frac{Sc_c}{\nu_f}\right)g\Phi' = 0, \tag{34}$$

$$\Psi'' - R\left(\frac{Sc_c}{\nu_f}\right)g\Psi' - Pe\left(\varepsilon_9\left(\Psi\Phi'' + \Psi'\Phi'\right) + \alpha_1\Phi''\right) = 0. \tag{35}$$

Case-2; (*n* ≠ 2) for a case of non-Newtonian model

The functions in the new forms will be:

$$u_w = \frac{e^{-\left(\frac{n-2}{n}\right)b^2\nu_f x}}{b}, \upsilon_w = \upsilon_o bH, U = e^{+\left(\frac{n-2}{n}\right)b^2\nu_f x}, W = \frac{R^{\left(\frac{n-1}{n-2}\right)}}{b\nu_f}, p_w = e^{-\left(\frac{\nu_f}{(bH)^2}\right)x}, \zeta = e^{+\left(\frac{\nu_f}{(bH)^2}\right)x}, \xi = \varrho = \pi = b\left(\nu_f\right)^{1-n} \text{ and } \eta = y\frac{\nu_f}{H} \tag{36}$$

Based on the previous results in Eq. (36), the system (22) to (28) will be stated as:

$$\left(f''\right)^{n-1} - \varepsilon_6\varepsilon_{10}(R)^{1-n}\left(-\left(\frac{n-2}{n}\right)f^2 + \varepsilon_{11}gf' + 2\lambda R^{\frac{1}{n-2}}h + M\left(\frac{\varepsilon_5}{\varepsilon_2}\right)f\sin^2(\Gamma)\right) = 0, \tag{37}$$

$$\left(h''\right)^{n-1} + \varepsilon_6\left(gh' - 2\lambda R^{\frac{3-2n}{n-2}}f + M\left(\frac{\varepsilon_5}{\varepsilon_2\varepsilon_{11}}\right)h\sin^2(\Gamma)\right) = 0, \tag{38}$$

$$\left(g''\right)^{n-1} - R^{\frac{n}{2}}\varepsilon_{13}\left(gg' + \frac{\varepsilon_{12}}{R\rho_{thnf}}E'\right) = 0, \tag{39}$$

$$\Theta'' + \left(\frac{RPr}{\varepsilon_4 + PrR_d}\right)\left(\varepsilon_3\varepsilon_8 g\Theta' - \left(\frac{\varepsilon_1\nu_f^{\,n}}{\Delta T}\right)g'^2\right) = 0, \tag{40}$$

$$\Phi'' + \left(\frac{N_t}{N_b}\right)\Theta'' - R\left(\frac{Sc_c}{\nu_f}\right)g\Phi' = 0, \tag{41}$$

$$\Psi'' - R\left(\frac{Sc_c}{\nu_f}\right)g\Psi' - Pe\left(\varepsilon_{14}\left(\Psi\Phi'' + \Psi'\Phi'\right) + \alpha_1\Phi''\right) = 0, \tag{42}$$

with the corresponding boundary conditions as follows:

$$\begin{aligned} &f = 1, g = 0, h = 0, E = 1, \Theta = 1, \Phi = 1, \Psi = 1 \rightarrow y = 0 \\ &f = 0, g = 1, h = 0, E = 0, \Theta = 0, \Phi = 0, \Psi = 0 \rightarrow y = H \end{aligned} \tag{43}$$

where the non-dimensional parameters in the above equations are $R = bH^2/\nu_f$ (Reynold's number), $\lambda = \Omega H^2/\nu_f$ (rotation parameter), $M = \sigma_f B_0^2 / b\rho_f$ (magnetic parameter), n (power-law index), Γ (inclination angle), $Pr = \nu_f/\alpha_f$ (Prandtl number), $R_d = 16\sigma^* T_\infty^3 / 3k^* \nu_f (\rho c_p)_f$ (radiation parameter), $Sc_c = \nu_f / D_B$ (Schmidt number), $N_t = \tau D_T \Delta T / \nu_f T_\infty$ (thermophoresis parameter), $N_b = \tau D_B \Delta C/\nu_f$ (Brownian motion parameter), $Sc_N = \nu_f / D_n$ (bioconvection Schmidt number), $Pe = \chi W_c / D_n$ (bioconvection Peclet number) and $\alpha_1 = N_\infty / (N_w - N_\infty)$ (microorganism difference parameter). The correlations of ternary hybrid nanofluid are presented as follow [9, 10]:

$$\begin{aligned}
&\varepsilon_1 = \frac{\mu_{thnf}}{\mu_f} = (1-\varphi_1)^{-2.5}(1-\varphi_2)^{-2.5}(1-\varphi_3)^{-2.5} \\
&\varepsilon_2 = \frac{\rho_{thnf}}{\rho_f} = \frac{\left((1-\varphi_1)\left[(1-\varphi_2)\left[(1-\varphi_3)\rho_f + \varphi_3\rho_3\right] + \varphi_2\rho_2\right] + \varphi_1\rho_1\right)}{\rho_f} \\
&\varepsilon_3 = \frac{(\rho c_p)_{thnf}}{(\rho c_p)_f} = \frac{\left((1-\varphi_1)\left[(1-\varphi_2)\left[(1-\varphi_3)(\rho c_p)_f + \varphi_3(\rho c_p)_3\right] + \varphi_2(\rho c_p)_2\right] + \varphi_1(\rho c_p)_1\right)}{(\rho c_p)_f} \\
&\varepsilon_4 = \frac{k_{thnf}}{k_{hnf}} = \frac{k_1 + 2k_{hnf} - 2\varphi_1(k_{hnf} - k_1)}{k_1 + 2k_{hnf} + \varphi_1(k_{hnf} - k_1)}; \frac{k_{hnf}}{k_{nf}} = \frac{k_2 + 2k_{nf} - 2\varphi_2(k_{nf} - k_2)}{k_2 + 2k_{nf} + \varphi_2(k_{nf} - k_2)}; \frac{k_{nf}}{k_f} = \frac{k_3 + 2k_f - 2\varphi_3(k_f - k_3)}{k_3 + 2k_f + \varphi_3(k_f - k_3)} \\
&\varepsilon_5 = \frac{\sigma_{thnf}}{\sigma_{hnf}} = \frac{(1+2\varphi_1)\sigma_1 + (1-2\varphi_1)\sigma_{hnf}}{(1-\varphi_1)\sigma_1 + (1+\varphi_1)\sigma_{hnf}}; \frac{\sigma_{hnf}}{\sigma_{nf}} = \frac{(1+2\varphi_2)\sigma_2 + (1-2\varphi_2)\sigma_{nf}}{(1-\varphi_2)\sigma_2 + (1+\varphi_2)\sigma_{nf}}; \frac{\sigma_{nf}}{\sigma_f} = \frac{(1+2\varphi_3)\sigma_3 + (1-2\varphi_3)\sigma_f}{(1-\varphi_3)\sigma_3 + (1+\varphi_3)\sigma_f}
\end{aligned} \tag{44}$$

where

$$\varepsilon_6 = \frac{1}{\nu_{thnf}}, \varepsilon_7 = (b\nu_f)^{3/2} \upsilon_o^2, \varepsilon_8 = \frac{\upsilon_o}{\nu_f}, \varepsilon_9 = \frac{1}{\sqrt{b\nu_f}}, \varepsilon_{10} = \frac{(\nu_f)^{n-3}}{\upsilon_o^2}, \varepsilon_{11} = \upsilon_o\nu_f, \varepsilon_{12} = \frac{1}{b\nu_f}, \varepsilon_{13} = (b\nu_f)^{\frac{(6-3n)}{2}}, \varepsilon_{14} = (b\nu_f)^{1-n} \tag{45}$$

The dimensionless forms of interest physical quantities are skin friction, Nusselt number, Sherwood number and microorganisms density number as shown in [2, 4, 44]:

$$\begin{aligned}
C_f &= \left(\frac{\varepsilon_1}{\varepsilon_2}\right)\nu_f^2 f'(0) \\
Nu &= -\varepsilon_4\left[1 + R_d\left(\frac{\nu_f}{\varepsilon_3}\right)\right]\Theta'(0) \\
Sh &= -\sqrt{\nu_f}\phi'(0) \\
Nn &= -\sqrt{\nu_f}\Psi'(0)
\end{aligned} \tag{46}$$

where $Re = H\, u_w / \nu_f$ is the Reynold number.

4. Results and Discussion

The model of THNF with gyrotactic microorganisms inside a microchannel is solved by using GTM technique. The effect of physical parameters on the characteristic of ternary hybrid nanofluid in the existence of solar radiation has been delineated in diagrams. The influence of nonhomogeneous distribution of nanoparticles and motile microorganisms has been considered in this study. The ternary hybrid nanofluid contains the (Cu, Fe_3O_4 and Al_2O_3) nanoparticles with water base fluid. Recently, using magnetic nanoparticles (Fe_3O_4) and non-magnetic nanoparticles (Cu and Al_2O_3) has mechanical features and physicochemical properties in nanotechnology and solar collectors [45, 18]. Thus, magnetic nanoparticles have high magnetic susceptibility and high saturation magnetization [17]. To enhance the performance of heat and mass transfer of the fluid, these nanoparticles are used as an effective nanomaterial in studies [4, 18, 45, 46]. In the present figures, the used parameters are $Pr = 6.9$ referring water base fluid [4, 17, 18], $R = 1$ [4, 19], $R_d = Sc_C = Sc_N = 0.1$ [18, 47, 48], $\lambda = 0.01$ [49, 50], $\Gamma = \pi/2$ [18, 47], $N_t = N_b = 0.5$ [48, 51], and $Pe = 1$ [2]. The characteristics of (H_2O) base fluid, (Cu, Fe_3O_4 and Al_2O_3) nanoparticles are shown in Table 1 [7, 10, 45].

Table 1. Thermophysical properties of H_2O, Cu, Fe_3O_4 and Al_2O_3.

Material	ρ (kg/m^3)	C_p $(J/kg.K)$	k $(W/m.K)$	σ (S/m)
Water (H_2O)	997.1	4179	0.613	0.05
Copper (Cu)	8933	385	401	5.96×10^7
Ferro (Fe_3O_4)	5180	670	9.7	0.74×10^6
Alumina (Al_2O_3)	3970	765	0.613	3.5×10^7

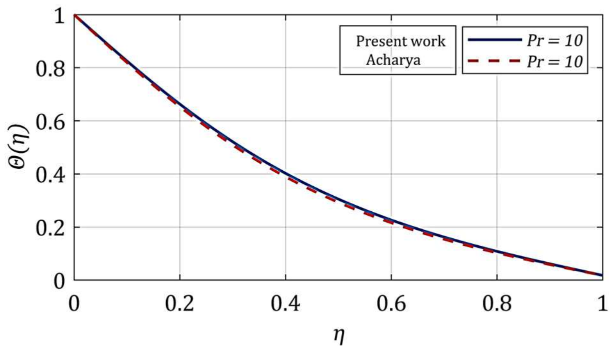

Fig. 2. Verification of temperature with Ref. [4] at $Pr = 10$ when $M = R = Pe = 1, N_t = N_b = 0.5,\ Sc = Sc_N = 0.1, R_d = 0.1, \lambda = 0.01, \Gamma = \pi / 2.$

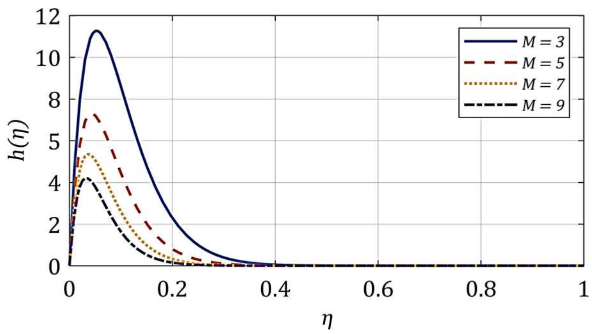

(a) Horizontal velocity against inclination angle when $Pr = 6.9, n = 2, R = Pe = 1, N_t = N_b = 0.5,$ $Sc_c = Sc_N = R_d = 0.1, \Gamma = \pi / 2, \lambda = 0.01$

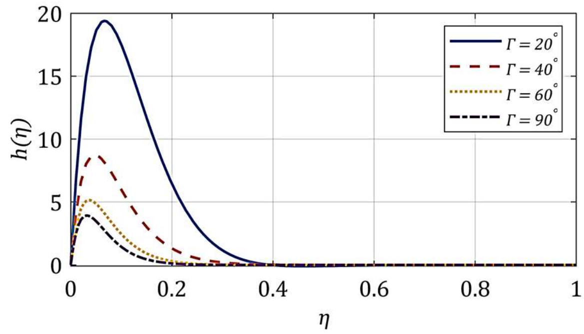

(b) Horizontal velocity against magnetic field when $Pr = 6.9, n = 2, R = Pe = 1, N_t = N_b = 0.5,$ $Sc_c = Sc_N = R_d = 0.1, M = 5, \lambda = 0.01$

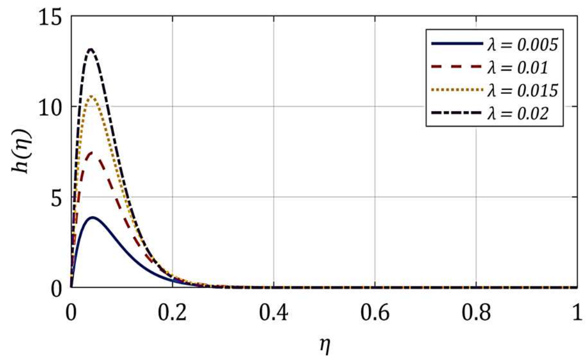

(c) Horizontal velocity against rotation parameter when $Pr = 6.9, n = 2, R = Pe = 1, N_t = N_b = 0.5,$ $Sc_c = Sc_N = R_d = 0.1, M = 5, \Gamma = \pi / 2$

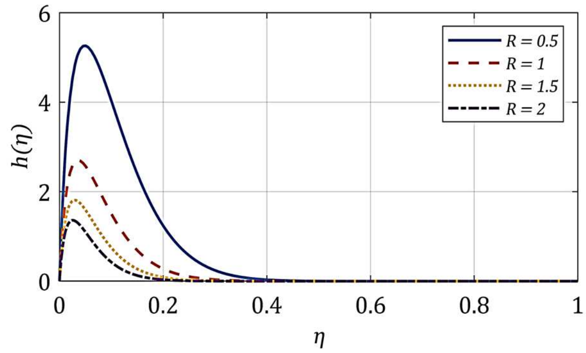

(d) Horizontal velocity against Reynold number when $Pr = 6.9, n = 2, Pe = 1, N_t = N_b = 0.5, M = 5,$ $Sc_c = Sc_N = R_d = 0.1, \Gamma = \pi / 2, \lambda = 0.01$

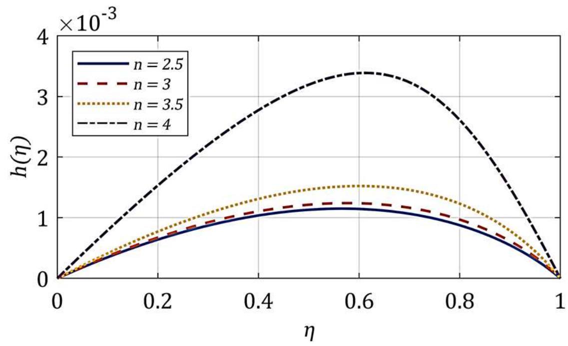

(e) Horizontal velocity against power law index when $Pr = 6.9, R = Pe = 1, N_t = N_b = 0.5,$ $Sc_c = Sc_N = R_d = 0.1, \Gamma = \pi / 2, \lambda = 0.01$

Fig. 3. Flow characteristics for different values of influential parameters.

Table 2. Comparing values of Nusselt number with variant in R and λ.

R	λ	Acharya [4]	Present work
2		1.6766	1.6767
3		1.7982	1.7964
4		1.9289	1.9285
	0	1.9605	1.9698
	0.5	1.9058	1.6061
	1	1.8463	1.8468

The verification of the numerical method is presented in Fig. 2. Therefore, the results reported by Acharya [4] are compared with the resulting data to validate the used methodology. As well as, according to Table 2, the Comparing values of the Nusselt number Nu with changing of Reynold number R and rotation parameter λ are performed in limiting case as in [4].

The results of Fig. 2 and Table 2 indicate that there is good agreement between the current analysis and the published results.

4.1. Velocity profiles

Variation in velocity profiles against the dominant parameters is examined in Fig. 3(a-e). Physically, arise in the values of magnetic field M resists the motion of ternary hybrid nanofluid due to generated Lorenz force. Therefore, the velocity of fluid diminishes with magnetic field as shown in Fig. 3(a). It is evident from Fig. 3(b) that higher values of inclination angle Γ and Reynold number R lead to decrement in the velocity because the gravity effect is diminished. The transverse velocity of the fluid increases by increasing values of rotation parameter λ as plotted in Fig. 3(c). In Fig. 3(d), from the definition of Reynold number, greater values of Reynold number correspond to increase in inertial force compared to the viscous force leading to decrement in the fluid velocity.

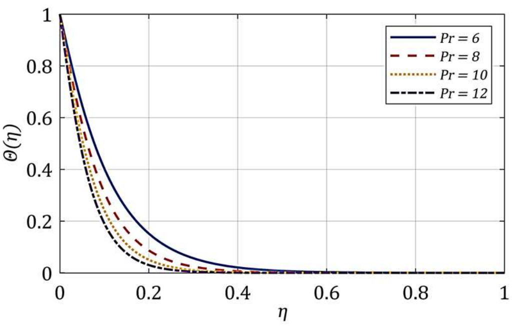

(a) Temperature profile against Prandtl number when $n = 2, R = Pe = 1, N_t = N_b = 0.5, \lambda = 0.01$ $Sc_c = Sc_N = R_d = 0.1, \Gamma = \pi / 2,$

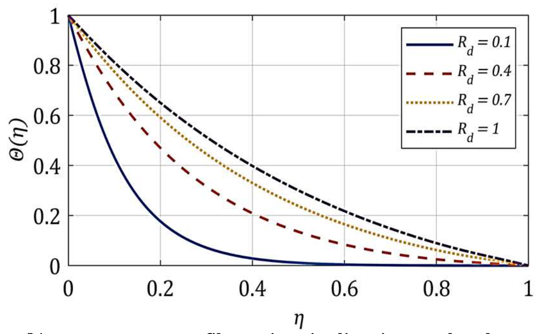

(b) Temperature profile against inclination angle when $Pr = 6.9, n = 2, R = Pe = 1, \lambda = 0.01$ $N_t = N_b = 0.5, \Gamma = \pi / 2$

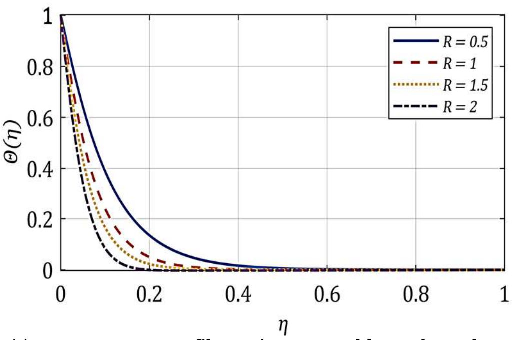

(c) Temperature profile against Reynold number when $Pr = 6.9, n = 2, Pe = 1, N_t = N_b = 0.5,$ $Sc_c = Sc_N = R_d = 0.1, \Gamma = \pi / 2, \lambda = 0.01$

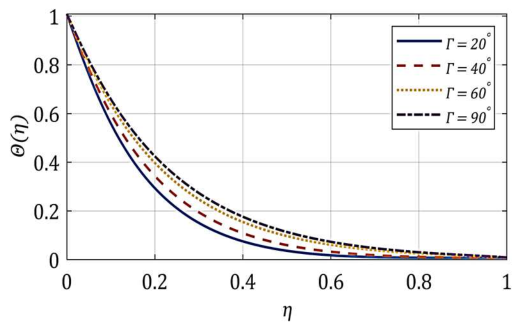

(d) Temperature profile against radiation parameter when $Pr = 6.9, R = Pe = 1, N_t = N_b = 0.5,$ $n = 2, Sc_c = Sc_N = R_d = 0.1, \lambda = 0.01$

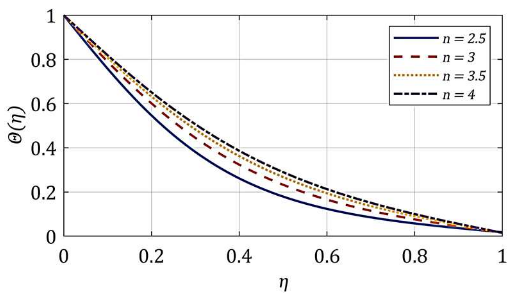

(e) Temperature profile against power-law index when $Pr = 6.9, R = Pe = 1, N_t = N_b = 0.5,$ $Sc_c = Sc_N = R_d = 0.1, \Gamma = \pi / 2, \lambda = 0.01$

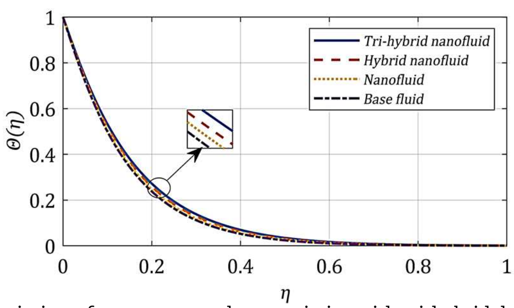

(f) Variation of temperature characteristics with tri-hybrid, hybrid nanofluid, nanofluid and base fluid when $Pr = 6.9, n = 2, R = Pe = 1, N_t = N_b = 0.5,$ $Sc_c = Sc_N = R_d = 0.1, \Gamma = \pi / 2, \lambda = 0.01$

Fig. 4. Thermal characteristics for different values of influential parameters.

4.2. Temperature profiles

The behavior of thermal field against the influential parameters is depicted in Fig. 4(a-e). Raising the values of Prandtl number leads to decrease the fluid temperature as displayed in Fig. 4(a). The system gained a high amount of heat with augment the radiation parameter R_d. So, the fluid temperature enhances with larger values of R_d as shown in Fig. 4(b). As well as, the temperature increases as inclination angle Γ and power-law index increase as shown in Fig. 4(d, e), respectively. The opposite observation is found in the case of Reynold number as depicted in Fig. 4(c). The thermal performance of ternary hybrid nanofluid, hybrid nanofluid, nanofluid and base fluid is observed in Fig. 4(f). The thermal performance is reached to more production in case of THNF.

4.3. Concentration profiles

The influence of the concentration field is graphically presented in Fig. 5. The concentration field slightly decreases by increasing of the Reynold number as shown in Fig. 5(a). Physically, increasing values of Schmidt number causes kinematic viscosity of the fluid which resists the Brownian diffusion. Therefore, raising the Schmidt number leads to reduce the concentration as displayed in Fig. 5(b).

4.4. Motile microorganism profiles

The impact of Peclet number Pe, Reynold number R and bioconvection Schmidt number Sc_N on motile microorganism is shown in Fig. 6(a-c). It was noticed that density of motile microorganism decreases for higher values of Pe, R and Sc_N.

4.5. Pressure profiles

The influence of magnetic field and inclination angle on fluid pressure is demonstrated in Fig. 7(a, b). In general, the maximum value of the pressure is attained at the lower surface and decays reaching to constant value at the upper surface with increasing the height of microchannel. At the surface of the channel, the fluid pressure raises with greater values of magnetic field and inclination angle.

In Tables 3 and 4, the effect of obtained parameters on C_f, Nu, Sh, Nn are displayed.

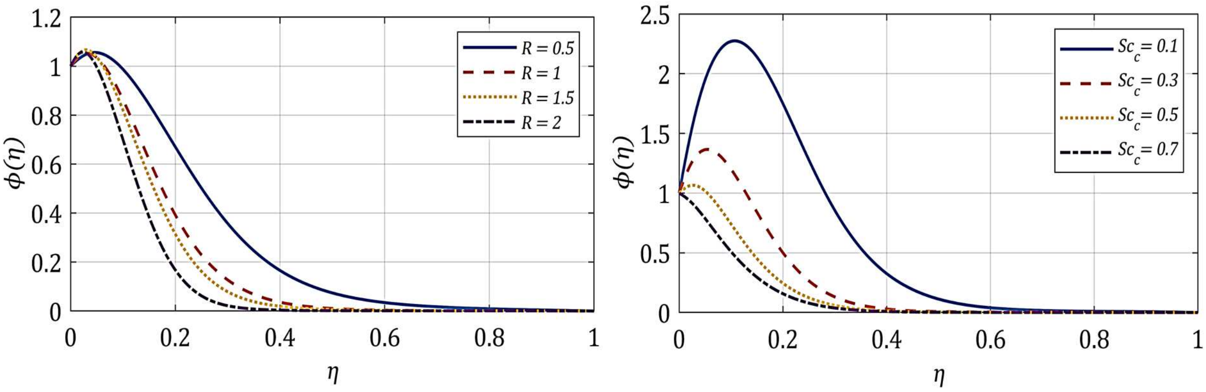

(a) Concentration profile against Reynold parameter when $Pr = 6.9, n = 2, Pe = 1, N_t = N_b = 0.5,$ $Sc_c = Sc_N = R_d = 0.1, \Gamma = \pi/2, \lambda = 0.01$

(b) Concentration profile against Schmidt number when $Pr = 6.9, R = Pe = 1, N_t = N_b = 0.5,$ $Sc_N = R_d = 0.1, n = 2, \Gamma = \pi/2, \lambda = 0.01$

Fig. 5. Concentration characteristics for different values of influential parameters.

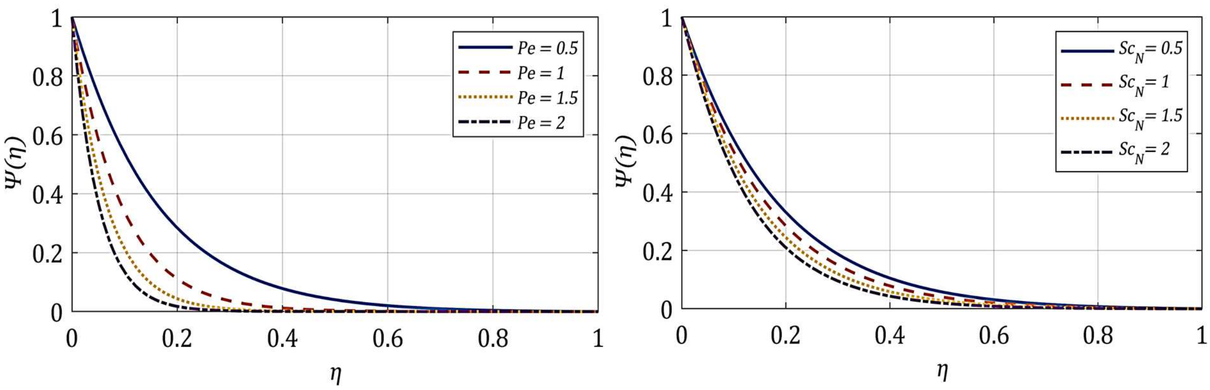

(a) Microorganism profile against Peclet number when $Pr = 6.9, n = 2, N_t = N_b = 0.5, \lambda = 0.01,$ $Sc_c = Sc_N = R_d = 0.1, \Gamma = \pi/2,$

(b) Microorganism profile against Schmidt number when $Pr = 6.9, n = 2, Pe = 1, N_t = N_b = 0.5,$ $Sc_c = R_d = 0.1, \Gamma = \pi/2, \lambda = 0.01$

Fig. 6. Motile microorganism characteristics for different values of influential parameters.

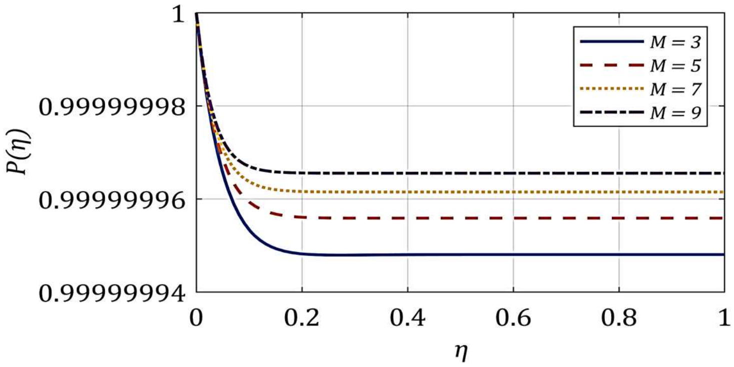

(a) Pressure profile against magnetic field when $Pr = 6.9, n = 2, R = Pe = 1, N_t = N_b = 0.5,\ Sc_c = Sc_N = R_d = 0.1, \Gamma = \pi / 2, \lambda = 0.01$

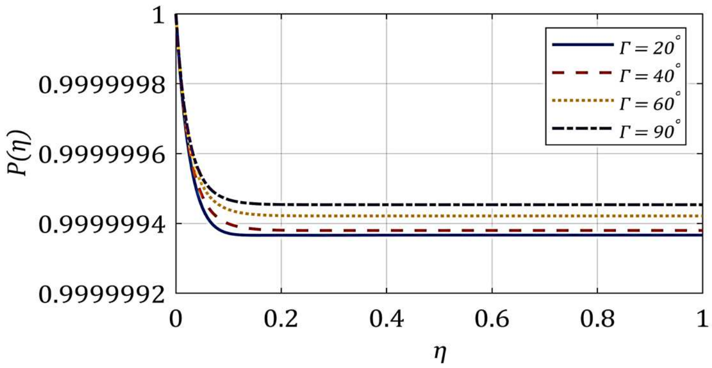

(b) Pressure profile against inclination angle when $Pr = 6.9, n = 2, R = Pe = 1,\ N_t = N_b = 0.5, Sc_c = Sc_N = R_d = 0.1, \lambda = 0.01$

Fig. 7. Fluid pressure for different values of influential parameters.

Table 3. Numerical values of skin friction, Nusselt number and Sherwood number.

R	λ	M	Pr	R_d	N_t	N_b	C_f	Nu	Sh
1							0.11444	1.18097	1.67587
3							0.13622	3.40398	2.37233
5							0.15634	6.30193	4.89617
	0						0.05994	2.23308	1.75159
	0.5						0.11445	0.71013	0.62550
	1						0.15374	0.59171	0.58822
		5					0.11717	2.24899	1.18880
		10					0.12528	2.07956	1.19639
		15					0.13305	1.93647	1.20705
			6				0.02468	2.45030	0.29412
			8				0.02468	3.03135	0.16038
			10				0.02468	3.56594	0.03653
				0.1			0.11717	0.59770	0.04358
				0.3			0.11717	4.01505	0.07461
				0.5			0.11717	8.13339	0.08595
					0.2		0.13591	2.74740	0.12744
					0.4		0.13591	2.74740	0.06943
					0.6		0.13591	2.74740	0.01142
						0.1	0.14578	3.03135	0.12557
						0.3	0.14578	3.03135	0.14440
						0.5	0.14578	3.03135	0.14816

Table 4. Tabulation of the microorganism density number with variants of R, Sc_N and Pe.

R	Sc_N	Pe	Nn
1			0.41484
3			0.56021
5			1.19947
	0.5		2.12456
	1		3.62209
	1.5		4.82152
		0.2	0.76983
		0.6	0.95937
		1	1.16508

Table 3 indicates that the skin friction coefficient is influenced by the Reynold number, rotation parameter, and magnetic field, as they impact the inertial and viscous forces in the hybrid nanofluid layers. The Nusselt number was influenced positively by the radiation parameter, Prandtl number, and Reynold number due to the thermal behavior of nanoparticles, whereas the rotation parameter and magnetic field have a negative effect on it. The parameters R, M, R_d, and N_b influence the mass transfer rate, leading to an increase in the Sherwood number. Conversely, the variables λ, Pr, and N_t have the opposite effect on this phenomenon. The microorganism density increases with higher values of R, Sc_N, and Pe, as seen in Table 4. The rise in parameter values is linked to the increase in diffusivity coefficient of the microorganisms, thus impacting the microorganism's density in the fluid.

5. Conclusion

The three-dimensional flow of THNF with microorganisms inside a micro-channel has been investigated in this study. The lower surface is stretchable, and the upper surface is revolving. The PDEs were nondimensionalized using GTM. A summary of the core finding is presented in the following points:

- Improving the value of rotation parameter and power-law index leads to increase in the velocity profile, but it decreases with magnetic parameter, inclination angle and Reynold number. The peak value of fluid velocity reduces by 33.33 % when the magnetic parameter is at range of $(3 \le M \le 5)$.
- The temperature field improves by raising the values of radiation parameter, power-law index and inclination angle. Furthermore, the temperature decays with augmentation values of Prandtl number and Reynold number.
- Concentration profile reduces with augmentation in Reynold number and Schmidt number, while it enhances by rising the Prandtl number.
- The microorganism minimizes with greater values of Peclet number, Reynold number and Schmidt number. The skin friction coefficient improves via Reynold number, rotation parameter and magnetic parameter. A percentage of 36.61 % for increasing in skin friction coefficient is predicted for a range $(1 \le \mathrm{Re} \le 5)$ of Reynold number.
- An increase in Pr, R and R_d gives magnification in Nusselt number, while the reverse phenomenon is noted with λ and M. The Sherwood number improves with the increment in R, M, R_d and N_b, while it diminishes with augmentation of λ, Pr and N_t. The motile microorganism number gets reduced with higher values of R, Sc_N and Pe.

The future work will concentrate on a novel ternary hybrid nanofluid combinations through new geometries with different flow conditions. Furthermore, the mathematical modeling may be solved using the Crank Nicholson Method (CNM) [52] or Adomian decomposition method (ADM) [53].

Author Contributions

A.S. Rashed: Review and editing. T.A. Mahmoud: Written and programing analysis. S.M. Mabrouk: methodology and editing. The manuscript was written through the contribution of all authors. All authors discussed the results, reviewed, and approved the final version of the manuscript.

Acknowledgments

Not applicable.

Conflict of Interest

The authors declared no potential conflicts of interest concerning the research, authorship, and publication of this article.

Funding

The authors received no financial support for the research, authorship, and publication of this article.

Data Availability Statements

The datasets generated and/or analyzed during the current study are available from the corresponding author on reasonable request.

Nomenclature

Latin symbols		Greek symbols	
a_1, a_2, a_3	Group parameters.	α_1	Microorganism difference parameter.
B_0	Uniform magnetic field (T).	Γ	Inclination angle (°).
ρc_p	Heat capacity (J kg^{-3} K^{-1}).	ΔT	Temperature difference parameter.
c_p	Specific heat (J kg^{-1} K).	η	Similarity variable.
D_T	Coefficient of thermophoresis diffusion (m^2 s^{-1}).	μ	Dynamic viscosity (m^2 s^{-1}).
D_B	Coefficient of Brownian diffusion (m^2 s^{-1}).	υ	Kinematic viscosity (m^2 s^{-1}).
D_n	Coefficient of microorganism's diffusion (m^2 s^{-1}).	ρ	Density (kg m^{-3}).
M	Magnetic parameter.	σ	Electric conductivity (S m^{-1}).
N_n	Microorganism density number.	σ^*	Stefan -Boltzmann Constant (5.67×10^{-8} W m^{-2} K^{-4}).
N_t	Thermophoresis parameter.	ϕ	Dimensionless concentration.
N_b	Brownian motion parameter.	χ	Chemotaxis constant.

Nu	Nusselt number.
Pr	Prandtl number.
R_d	Radiation parameter.
R	Reynolds number.
Sc	Schmidt number.
Sh	Sherwood number.
u^*, v^*, w^*	Velocity components (m s^{-1}).
W_c	Swimming speed (m s^{-1}).
x, y, z	Cartesian coordinates (m).
Ψ	Dimensionless gyrotactic microorganisms.
Ω	Rotation velocity.

Subscript

f	Base fluid.
hnf	Hybrid nanofluid.
$thnf$	Ternary hybrid nanofluid.

Superscript

$()'$	Differentiation with respect to η.

References

[1] Obaideen, K., Nooman AlMallahi, M., Alami, A.H., Ramadan, M., Abdelkareem, M.A., Shehata, N., Olabi, A.G., On the contribution of solar energy to sustainable developments goals: Case study on mohammed bin rashid al maktoum solar park, *International Journal of Thermofluids*, 12, 2021, 100123.

[2] Farooq, U., Waqas, H., Shah, Z., Kumam, P., Deebani, W., On unsteady 3d bio-convection flow of viscoelastic nanofluid with radiative heat transfer inside a solar collector plate, *Scientific Reports*, 12, 2022, 2952.

[3] Acharya, N., Das, K., Kundu, P.K., Effects of aggregation kinetics on nanoscale colloidal solution inside a rotating channel, *Journal of Thermal Analysis and Calorimetry*, 138, 2019, 461-477.

[4] Acharya, N., On the flow patterns and thermal behaviour of hybrid nanofluid flow inside a microchannel in presence of radiative solar energy, *Journal of Thermal Analysis and Calorimetry*, 141, 2020, 1425-1442.

[5] Fakour, M., Vahabzadeh, A., Ganji, D.D., Scrutiny of mixed convection flow of a nanofluid in a vertical channel, *Case Studies in Thermal Engineering*, 4, 2014, 15-23.

[6] Acharya, N., Das, K., Kundu, P., Effects of aggregation kinetics on nanoscale colloidal solution inside a rotating channel: A thermal framework, *Journal of Thermal Analysis and Calorimetry*, 138, 2019, 461-477.

[7] Noreen, S., Farooq, U., Waqas, H., Fatima, N., Alqurashi, M.S., Imran, M., Akgül, A., Bariq, A., Comparative study of ternary hybrid nanofluids with role of thermal radiation and cattaneo-christov heat flux between double rotating disks, *Scientific Reports*, 13, 2023, 7795.

[8] Khan, S.A., Hayat, T., Alsaedi, A., Thermal conductivity performance for ternary hybrid nanomaterial subject to entropy generation, *Energy Reports*, 8, 2022, 9997-10005.

[9] Bilal, M., Ullah, I., Alam, M.M., Weera, W., Galal, A.M., Numerical simulations through pcm for the dynamics of thermal enhancement in ternary mhd hybrid nanofluid flow over plane sheet, cone, and wedge, *Symmetry*, 14, 2022, 2419.

[10] Alqawasmi, K., Alharbi, K.A.M., Farooq, U., Noreen, S., Imran, M., Akgül, A., Kanan, M., Asad, J., Numerical approach toward ternary hybrid nanofluid flow with nonlinear heat source-sink and fourier heat flux model passing through a disk, *International Journal of Thermofluids*, 18, 2023, 100367.

[11] Mohanty, D., Mahanta, G., Shaw, S., Irreversibility and thermal performance of nonlinear radiative cross-ternary hybrid nanofluid flow about a stretching cylinder with industrial applications, *Powder Technology*, 433, 2024, 119255.

[12] Waqas, H., Farooq, U., Ibrahim, A., Kamran Alam, M., Shah, Z., Kumam, P., Numerical simulation for bioconvectional flow of burger nanofluid with effects of activation energy and exponential heat source/sink over an inclined wall under the swimming microorganisms, *Scientific Reports*, 11, 2021, 14305.

[13] Alharbi, F.M., Naeem, M., Zubair, M., Jawad, M., Jan, W.U., Jan, R., Bioconvection due to gyrotactic microorganisms in couple stress hybrid nanofluid laminar mixed convection incompressible flow with magnetic nanoparticles and chemical reaction as carrier for targeted drug delivery through porous stretching sheet, *Molecules*, 26, 2021, 3954.

[14] Shi, Q.-H., Hamid, A., Khan, M.I., Kumar, R.N., Gowda, R.J.P., Prasannakumara, B.C., Shah, N.A., Khan, S.U., Chung, J.D., Numerical study of bio-convection flow of magneto-cross nanofluid containing gyrotactic microorganisms with activation energy, *Scientific Reports*, 11, 2021, 16030.

[15] Rashed, A.S., Mahmoud, T.A., Kassem, M.M., Behavior of nanofluid with variable brownian and thermal diffusion coefficients adjacent to a moving vertical plate, *Journal of Applied and Computational Mechanics*, 7, 2021, 1466-1479.

[16] Rashed, A., Mahmoud, T., Kassem, M., Analysis of homogeneous steady state nanofluid surrounding cylindrical solid pipes, *The Egyptian International Journal of Engineering Sciences and Technology*, 31, 2020, 71-82.

[17] Mabrouk, S.M., Mahmoud, T.A., Kabeel, A.E., Rashed, A.S., Influence of power-law index and hybrid-nanoparticles concentrations on the behavior of non-newtonian hybrid nanofluid inside water solar collector, *Modern Physics Letters B*, 38, 2023, 2350226.

[18] Mabrouk, S., Mahmoud, T., Kabeel, A.E., Rashed, A., Essa, F., Thermal and entropy behavior of sustainable solar energy in water solar collector due to non-newtonian power-law hybrid nanofluid, *Frontiers in Energy Research*, 11, 2023, 1220587.

[19] Abdollahi, S.A., Alizadeh, A.A., Esfahani, I.C., Zarinfar, M., Pasha, P., Investigating heat transfer and fluid flow betwixt parallel surfaces under the influence of hybrid nanofluid suction and injection with numerical analytical technique, *Alexandria Engineering Journal*, 70, 2023, 423-439.

[20] Waqas, H., Khan, S.A., Khan, S.U., Khan, M.I., Kadry, S., Chu, Y.-M., Falkner-skan time-dependent bioconvrction flow of cross nanofluid with nonlinear thermal radiation, activation energy and melting process, *International Communications in Heat and Mass Transfer*, 120, 2021, 105028.

[21] Rashed, A.S., Analysis of (3+1)-dimensional unsteady gas flow using optimal system of lie symmetries, *Mathematics and Computers in Simulation*, 156, 2019, 327-346.

[22] Rashed, A.S., Nasr, E.H., Kassem, M.M., Similarity analysis of mass and heat transfer of fhd steady flow of nanofluid incorporating magnetite nanoparticles (fe3o4), *East African Scholars Journal of Engineering and Computer Sciences*, 3, 2020, 54-63.

[23] Rashed, A.S., Mabrouk, S.M., Wazwaz, A.-M., Unsteady three-dimensional laminar flow over a submerged plate in electrically conducting fluid with applied magnetic field, *Waves in Random and Complex Media*, 33, 2023, 505-524.

[24] Rashed, A.S., Mabrouk, S.M., Wazwaz, A.-M., Forward scattering for non-linear wave propagation in (3 + 1)-dimensional jimbo-miwa equation using singular manifold and group transformation methods, *Waves in Random and Complex Media*, 32, 2022, 663-675.

[25] Saleh, R., Rashed, A.S., Wazwaz, A.-M., Plasma-waves evolution and propagation modeled by sixth order ramani and coupled ramani equations using symmetry methods, *Physica Scripta*, 96, 2021, 085213.

[26] Sarma, N., Paul, A., Thermophoresis and brownian motion influenced bioconvective cylindrical shaped ag–cuo/h2o ellis hybrid nanofluid flow along a radiative stretched tube with inclined magnetic field, *BioNanoScience*, 2023, DOI: 10.1007/s12668-023-01280-1.

[27] Paul, A., Sarma, N., Patgiri, B., Mixed convection of shear-thinning hybrid nanofluid flow across a radiative unsteady cone with suction and slip effect, *Materials Today Communications*, 37, 2023, 107522.

[28] Rafique, K., Mahmood, Z., Khan, U., Eldin, S.M., Oreijah, M., Guedri, K., Khalifa, H.A.E.-W., Investigation of thermal stratification with velocity slip and variable viscosity on mhd flow of al2o3–cu–tio2/h2o nanofluid over disk, *Case Studies in Thermal Engineering*, 49, 2023, 103292.

[29] Paul, A., Sarma, N., Patgiri, B., Thermal and mass transfer analysis of casson-maxwell hybrid nanofluids through an unsteady horizontal cylinder with variable thermal conductivity and arrhenius activation energy, *Numerical Heat Transfer, Part A: Applications*, 2023, DOI: 10.1080/10407782.2023.2297000.

[30] Mahmood, Z., Eldin, S.M., Rafique, K., Khan, U., Numerical analysis of mhd tri-hybrid nanofluid over a nonlinear stretching/shrinking sheet with heat generation/absorption and slip conditions, *Alexandria Engineering Journal*, 76, 2023, 799-819.

[31] Islam, S., Rana, B.M.J., Parvez, M.S., Hossain, M.S., Rahman, M.M., Electroosmotic flow in ternary (tio2-sio2-al2o3) blood-based sutterby nanomaterials with bio-active mixers, *International Journal of Thermofluids*, 18, 2023, 100363.

[32] Islam, S., Rana, B.M.J., Parvez, M.S., Hossain, M.S., Mazumder, M., Roy, K.C., Rahman, M.M., Dynamics of chemically reactive carreau nanomaterial flow along a stretching riga plate with active bio-mixers and arrhenius catalysts, *Heliyon*, 9, 2023, e21727.

[33] Rana, B., Arifuzzaman, S.M., Islam, S., Reza-E-Rabbi, S., Hossain, K., Ahmmed, S., Khan, M., Swimming of microbes in entropy optimized nano-bioconvective flow of prandtl–erying fluid, *Heat Transfer*, 51, 2022, 5497-5531.

[34] Rana, B.M.J., Arifuzzaman, S.M., Islam, S., Reza-E-Rabbi, S., Al-Mamun, A., Mazumder, M., Roy, K.C., Khan, M.S., Swimming of microbes in blood flow of nano-bioconvective williamson fluid, *Thermal Science and Engineering Progress*, 25, 2021, 101018.
[35] Islam, M.S., Islam, S., Siddiki, M.N.A.A., Numerical simulation with sensitivity analysis of mhd natural convection using cu-tio2-h2o hybrid nanofluids, *International Journal of Thermofluids*, 20, 2023, 100509.
[36] Smrity, A.M.A., Yin, P., Design and performance evaluation of pulsating heat pipe using metallic nanoparticles based hybrid nanofluids, *International Journal of Heat and Mass Transfer*, 218, 2024, 124773.
[37] Jamshed, W., Sirin, C., Selimefendigil, F., Shamshuddin, M.D., Altowairqi, Y., Eid, M.R., Thermal characterization of coolant maxwell type nanofluid flowing in parabolic trough solar collector (ptsc) used inside solar powered ship application, *Coatings*, 11, 2021, 1552.
[38] Rashed, A.S., Kassem, M.M., Group analysis for natural convection from a vertical plate, *Journal of Computational and Applied Mathematics*, 222, 2008, 392-403.
[39] Kassem, M., Group solution for unsteady free-convection flow from a vertical moving plate subjected to constant heat flux, *Journal of Computational and Applied Mathematics*, 187, 2006, 72-86.
[40] Sheikholeslami, M., Rokni, H.B., Simulation of nanofluid heat transfer in presence of magnetic field: A review, *International Journal of Heat and Mass Transfer*, 115, 2017, 1203-1233.
[41] Sojoudi, A., Mazloomi, A., Saha, S.C., Gu, Y.T., Similarity solutions for flow and heat transfer of non-newtonian fluid over a stretching surface, *Journal of Applied Mathematics*, 2014, 2014, 718319.
[42] Abd-el-Malek, M.B., Helal, M.M., Similarity solutions for magneto-forced-unsteady free convective laminar boundary-layer flow, *Journal of Computational and Applied Mathematics*, 218, 2008, 202-214.
[43] Moran, M.J., Gaggioli, R.A., A new systematic formalism for similarity analysis, *Journal of Engineering Mathematics*, 3, 1969, 151-162.
[44] Jamshed, W., Eid, M.R., Azeany Mohd Nasir, N.A., Nisar, K.S., Aziz, A., Shahzad, F., Saleel, C.A., Shukla, A., Thermal examination of renewable solar energy in parabolic trough solar collector utilizing maxwell nanofluid: A noble case study, *Case Studies in Thermal Engineering*, 27, 2021, 101258.
[45] Jamshed, W., Aziz, A., A comparative entropy based analysis of cu and fe3o4/methanol powell-eyring nanofluid in solar thermal collectors subjected to thermal radiation, variable thermal conductivity and impact of different nanoparticles shape, *Results in Physics*, 9, 2018, 195-205.
[46] Nezafat, Z., Nasrollahzadeh, M., Biosynthesis of cu/fe3o4 nanoparticles using alhagi camelorum aqueous extract and their catalytic activity in the synthesis of 2-imino-3-aryl-2,3-dihydrobenzo[d]oxazol-5-ol derivatives, *Journal of Molecular Structure*, 1228, 2021, 129731.
[47] Ghadikolaei, S.S., Hosseinzadeh, K., Ganji, D.D., Jafari, B., Nonlinear thermal radiation effect on magneto casson nanofluid flow with joule heating effect over an inclined porous stretching sheet, *Case Studies in Thermal Engineering*, 12, 2018, 176-187.
[48] Azam, M., Shakoor, A., Rasool, H.F., Khan, M., Numerical simulation for solar energy aspects on unsteady convective flow of mhd cross nanofluid: A revised approach, *International Journal of Heat and Mass Transfer*, 131, 2019, 495-505.
[49] Sheikholeslami, M., Ganji, D.D., Numerical investigation for two phase modeling of nanofluid in a rotating system with permeable sheet, *Journal of Molecular Liquids*, 194, 2014, 13-19.
[50] Sheikholeslami, M., Hatami, M., Ganji, D.D., Nanofluid flow and heat transfer in a rotating system in the presence of a magnetic field, *Journal of Molecular Liquids*, 190, 2014, 112-120.
[51] Ghobadi, A.H., Hassankolaei, M.G., Numerical treatment of magneto carreau nanofluid over a stretching sheet considering joule heating impact and nonlinear thermal ray, *Heat Transfer—Asian Research*, 48, 2019, 4133-4151.
[52] Ghasemi, S.E., Hatami, M., Hatami, J., Sahebi, S.A.R., Ganji, D.D., An efficient approach to study the pulsatile blood flow in femoral and coronary arteries by differential quadrature method, *Physica A: Statistical Mechanics and its Applications*, 443, 2016, 406-414.
[53] Thumma, T., Mishra, S.R., Effect of nonuniform heat source/sink, and viscous and joule dissipation on 3d eyring–powell nanofluid flow over a stretching sheet, *Journal of Computational Design and Engineering*, 7, 2020, 412-426.

ORCID iD

Ahmed S. Rashed https://orcid.org/0000-0001-7800-2768
Tarek A. Mahmoud https://orcid.org/0000-0001-8846-0877
Samah M. Mabrouk https://orcid.org/0000-0003-1877-3944

How to cite this article: Rashed A.S., Mahmoud T.A., Mabrouk S.M. Enhanced Flow and Temperature Profiles in Ternary Hybrid Nanofluid with Gyrotactic Microorganisms: A Study on Magnetic Field, Brownian Motion, and Thermophoresis Phenomena, *J. Appl. Comput. Mech.*, 10(3), 2024, 597–609. https://doi.org/10.22055/jacm.2024.45899.4427